Environmental Science Nano

PAPER

View Article Online
View Journal | View Issue

Cite this: *Environ. Sci.: Nano*, 2016, 3, 567

Aggregation and sedimentation of magnetite nanoparticle clusters†

P. J. Vikesland,*[abc] R. L. Rebodos,[ab] J. Y. Bottero,[bc] J. Rose[bc] and A. Masion[bc]

Received 16th July 2015,
Accepted 22nd March 2016

DOI: 10.1039/c5en00155b

rsc.li/es-nano

Magnetite nanoparticles are redox active constituents of subsurface and corrosive environments. In this study, we characterized the aggregation and sedimentation behavior of well characterized magnetite nanoparticle clusters using dynamic light scattering (DLS), UV-vis-NIR spectroscopy, and small angle X-ray scattering (SAXS). Both unfunctionalized (NaOH-magnetite) and tetramethylammonium hydroxide (TMAOH-magnetite) surface functionalized nanoparticle clusters were employed. TMAOH-magnetite has a slightly smaller primary nanoparticle radius as determined by TEM (4 ± 0.7 nm *vs.* 5 ± 0.8 for NaOH-magnetite) and a smaller initial DLS determined cluster radius (<30 nm *vs.* 100–200 nm for NaOH-magnetite). Interestingly, in spite of its smaller initial nanoparticle cluster size, TMAOH-magnetite undergoes sedimentation more rapidly than NaOH-magnetite. This behavior is consistent with the more rapid aggregation of the smaller TMAOH-magnetite clusters as well as their lower fractal dimension, as determined by SAXS. This study illustrates that both nanoparticle cluster size and fractal dimension should be carefully considered when considering the environmental transport and fate of highly aggregated nanoparticles.

Nano impact

Nanoparticles are often highly aggregated when present in natural water systems. This paper illustrates that the fractal structure of these aggregated (or agglomerated) nanoparticle clusters can affect both cluster–cluster aggregation as well as cluster sedimentation. Using a combination of dynamic light scattering, UV-vis based sedimentation curves, and small angle X-ray scattering we illustrate that cluster size and fractal dimension should be collectively considered when evaluating the fate of highly aggregated nanomaterials. While our study focused explicitly on magnetite nanoparticles, the results are relevant to any other highly aggregated (or agglomerated) system.

Introduction

The mixed valence iron oxide magnetite (Fe_3O_4) is commonly found in subsurface and highly corrosive environments.[1–5] Over the past fifteen years there has been growing interest in the application of nanoscale magnetite for contaminated groundwater treatment and as a sorbent of metalloid contaminants due to its reductive capacity, high surface area, and superparamagnetic properties.[6–12] Magnetite has an inverse spinel crystal structure with a unit cell comprised of 32 O^{2-} anions, 16 Fe^{3+} cations, and 8 Fe^{2+} cations. Half of the Fe^{3+} ions are tetrahedrally (tet) coordinated, while the other half and all of the Fe^{2+} are octahedrally (oct) coordinated resulting in a $(Fe_8^{3+})_{tet}(Fe_8^{3+}Fe_8^{2+})_{oct}O_{32}$ unit cell. The adjacent positioning of Fe^{3+} and Fe^{2+} cations in the octahedral layer enables electron hopping due to d orbital overlap between iron atoms.[13]

In aqueous suspensions, magnetite readily aggregates due to a combination of Lifschitz–van der Waals and magnetic forces.[6,9,14] The size of these aggregated nanoparticle clusters can be considerable (potentially >1 μm) and thus cluster formation not only affects magnetite transport and delivery, but may also affect reactivity due to the loss of the specific activity of an individual nanoparticle.[10,15–18] Aggregation events between individual nanoparticles or between nanoparticle clusters can result either in the formation of irreversibly bound aggregates produced by close contact or in the formation of reversibly bound agglomerates that can be broken by sonication or other mixing processes.[19] Whether particles aggregate irreversibly or reversibly is dependent upon the relative magnitudes of the attractive and repulsive forces between the nanoparticles. Because of the challenges associated with experimentally differentiating aggregates from agglomerates

[a] *Department of Civil and Environmental Engineering and Institute for Critical Technology and Applied Science (ICTAS), Virginia Tech, Blacksburg, VA, USA. E-mail: pvikes@vt.edu*
[b] *Center for the Environmental Implications of Nanotechnology (CEINT), Duke University, Durham, NC, USA*
[c] *International Center for the Environmental Implications of Nanotechnology (iCEINT), Aix-en-Provence, France*

† Electronic supplementary information (ESI) available. Nanoparticle concentration calculations; additional figures and summary tables. See DOI: 10.1039/c5en00155b

and inconsistencies in the literature as to how these terms should be used,[20] herein, we refer to irreversibly bound masses of nanoparticles as nanoparticle clusters and the physical process bringing such clusters together as aggregation.

Nanoparticle clusters produced by aggregation processes generally can be considered self-similar fractal structures[19,21–23] that can be defined in terms of a fractal dimension (d_f) that is the power to which the radius of a nanoparticle cluster (R) is raised such that it scales with mass (m):[24]

$$m \alpha R^{d_f} \quad (1)$$

The fractal dimension of a cluster can depend on the mechanism by which the aggregation process occurs – namely whether it is diffusion limited cluster aggregation (DLCA) or reaction limited cluster aggregation (RLCA).[19,24,25] DLCA or fast aggregation occurs when no net repulsive force is experienced by the particles or clusters. Under these conditions the aggregation rate is solely dependent on the diffusion of the clusters to one another. At high electrolyte concentrations, coagulation in the DLCA regime leads to structures of low fractal dimension (*i.e.*, loose and open aggregates; $d_f \approx 1.7–1.8$).[26] For RLCA or slow aggregation, however, additional repulsive forces prevent the clusters from coagulating as readily. The formation of aggregated nanoparticle clusters is therefore dictated by the probability of the clusters adhering to one another. Structures formed by RLCA are more compact and have higher fractal dimensions ($d_f \approx 2.1–2.2$).[26] Because of these differences d_f is often used as a measure to evaluate cluster formation mechanisms.[24]

Light scattering methods have commonly been used to characterize aggregation processes.[27–29] Dynamic light scattering (DLS) is a technique in which temporal fluctuations of scattered light are analyzed to obtain the diffusion coefficient and consequently the hydrodynamic diameter of a given sample. Being a non-invasive technique, DLS was employed herein to characterize the aggregation behavior of magnetite produced both in the presence of tetramethylammonium hydroxide (TMAOH) and in its absence (TMAOH-magnetite and NaOH-magnetite, respectively). An inherent limitation of DLS, however, is that the method requires samples to have low particle concentrations to prevent multiple scattering events from occurring that can lead to inaccurate measurements. Given this restriction, UV-vis-NIR spectroscopy was also utilized to study the aggregation and sedimentation of magnetite at higher particle concentrations. These studies were achieved by monitoring changes in incident light intensity as it passes through a given sample over time. In addition, small angle X-ray scattering (SAXS) was used to probe the smallest nanoparticle sizes as well as the fractal structure of the nanoparticle clusters.

As discussed herein, the aggregation and sedimentation of magnetite clusters was found to be a function of the magnetite surface coating and the fractal dimension of the clusters. This work has relevance not only to studies of magnetite and other iron containing materials, but also any other highly aggregated nanomaterial. As we demonstrate, the fractal dimension of a cluster must be considered when evaluating nanomaterial aggregation and sedimentation in aquatic systems.

Experimental methods

Reagents

Reagent grade chemicals were used without additional purification for all experiments. The following chemicals were used for magnetite synthesis: ferrous chloride tetrahydrate ($FeCl_2 \cdot 4H_2O$; ICN Biomedicals), ferric chloride ($FeCl_3$ anhydrous; Fisher Scientific), sodium hydroxide (NaOH; Fisher Scientific; ≥98.5%), sodium chloride (NaCl; Fisher Scientific), and tetramethylammonium hydroxide pentahydrate ($TMAOH \cdot 5H_2O$; Fisher Scientific). All solutions used in the experiments were produced using de-aerated, deionized water (>18.1 MΩ cm) made by boiling for 30 minutes and then sparging with either argon or nitrogen gas for at least 30 minutes while boiling continued. De-aerated water was removed from the heating source, capped, transferred to an anaerobic glovebox (95% N_2/5% H_2; Coy Laboratory Products) and allowed to cool.

Magnetite synthesis

Magnetite nanoparticles were synthesized using a co-precipitation method adapted from Vayssières, *et al.*[30] In brief, in the anaerobic glovebox a mixture of 0.1 M $FeCl_2$ and 0.2 M $FeCl_3$ was added drop-wise (~1 drop per s) to a well-mixed solution of 1 M NaOH and 1 M NaCl. The final ratio of iron solution to base solution was kept at 3 : 2 to maintain the pH above 12. Polypropylene containers were used to avoid silicate leaching from glass vessels because of the high pH synthesis conditions. Excess salts were removed by magnetically separating the precipitated nanoparticles and by rinsing with argon-purged, deionized water until the supernatant pH was in the 7–8.5 range. TMAOH functionalized nanoparticles were synthesized using the same co-precipitation method except 1 M TMAOH was used instead of 1 M NaOH. Prepared magnetite stocks were stored in the anaerobic glovebox for periods up to 2 months. The mass concentration of a magnetite stock was gravimetrically determined in triplicate by drying 2 mL of slurry in a 75 °C oven. The final mass of dried sample was converted into an equivalent magnetite mass using the $Fe_3O_4/\gamma\text{-}Fe_2O_3$ gravimetric ratio and assuming 100% conversion of Fe_3O_4 into $\gamma\text{-}Fe_2O_3$.

Characterization of magnetite powders

The morphology and size of nanoparticulate magnetite were characterized using a Philips 420 T TEM operated at 100 keV. Particle slurries were mounted on carbon coated TEM grids (Electron Microscopy Science, Hartfield, PA) and dried in an aerobic environment for a minimum of 48 hours. Collected images were digitally transferred using a slow scan 3086 × 2056 pixel camera. The magnetite particle size was determined by analysis of collected TEM images using the ImageJ

software package (NIH, Bethesda, MD). High resolution transmission electron microscope (HRTEM) images were obtained using a FEI Titan scanning/transmission electron microscope (S/TEM) operated at 200 kV. Copper grids (400 mesh) with an ultrathin carbon film on a holey carbon support (Ted Pella, Inc.) were selected for samples investigated with the HRTEM. A representative selection of particle images was obtained from multiple sites on each grid.

Small angle X-ray scattering (SAXS)

SAXS experiments were conducted on the ID-02 beamline at the ESRF in Grenoble, France. Collected scattering curves were evaluated to determine both the nanoparticle size as well as the fractal dimension (d_f) of the magnetite clusters. A q range of $10^{-0.8}$–$10^{-2.2}$ Å^{-1} was probed with q defined as the wave vector modulus:

$$q = \frac{4\pi}{\lambda}\sin(\Theta) \quad (2)$$

where λ is 0.1 nm (12.4 keV), and 2Θ is the angle between the incident X-ray beam and the detector. A complete description of the data treatment can be found elsewhere.[31,32]

Determination of magnetite cluster–cluster aggregation kinetics

The aggregation behavior of the synthesized magnetite nanoparticle suspensions was studied using an ALV CGS-3 system and established protocols.[33,34] This system employs a 22 mW HeNe Laser, an APD-based single photon detector, and an ALV-5000/EPP correlator. The initial size and electrolyte-induced growth of the magnetite clusters were determined by cumulant analysis of dynamic light scattering (DLS) data collected at a 90° scattering angle every 15 seconds for a period of 30–60 minutes.

All DLS measurements were conducted at 25 °C and unless otherwise specified at pH = 8.0 ± 0.5. Each sample for analysis was placed in a new prewashed glass vial that was rinsed with filtered (Whatman nylon membrane, 0.2 μm), deionized water prior to the addition of suspension. Stock solutions of NaCl, $MgCl_2$, $CaCl_2$, and $FeCl_2$ were prepared using reagent grade salts and deaerated, deionized water. The solutions were double filtered with 0.1 μm Whatman nylon membrane and Anodisc membrane filters. To determine the effect of each electrolyte on magnetite cluster aggregation, known volumes of salt solution, corresponding to the desired salt concentration, were added to the pre-sonicated suspensions. All vials were vortex mixed for approximately five seconds upon salt addition to ensure adequate mixing.

Determination of magnetite cluster sedimentation rates

Magnetite cluster sedimentation was monitored using a Varian Cary 5000 UV-vis-NIR spectrophotometer. Magnetite suspensions with concentrations ranging from 0.22–22 mM (50–500 mg L^{-1}) were prepared inside the anaerobic glovebox by diluting a sonicated (FS204 Sonicator Bath, Fisher Scientific) magnetite stock. The dilute suspension was then sonicated for an additional 3 minutes prior to transferring a 3 mL aliquot to a quartz cuvette sealed with a rubber septum. Outside the glovebox, a syringe was used to add a given volume of deaerated 0.1 M NaCl to the magnetite suspension to vary ionic strength and induce sedimentation. UV-vis-NIR spectra were periodically obtained between 200 and 1350 nm for periods up to 60 minutes. In some experiments, measurements at 15 second intervals were obtained at a fixed wavelength of 508 nm for periods up to 60 minutes. Baseline corrections employing distilled deionized water were performed prior to sample analysis.

Results and discussion

Magnetite primary particle characterization

As shown in Fig. S1† and as described previously,[14] analysis of TEM images indicated that NaOH-magnetite has a particle radius of 5.0 ± 0.8 nm, while TMAOH-magnetite is smaller with a particle radius of 4.0 ± 0.7 nm. XRD, FTIR, and Raman measurements confirmed that the particles consist of magnetite/maghemite, and Scherer analyses of the collected X-ray diffractograms were consistent with the relative sizes determined *via* TEM. FTIR measurements for TMAOH-magnetite indicate that a layer of adsorbed tetramethyl ammonium (TMA^+) cations exists at the surface of this nanomaterial. TEM images for NaOH-magnetite (Fig. 1a) and TMAOH-magnetite (Fig. 1b) illustrate the smaller size of TMAOH-magnetite. Furthermore, as shown by the lattice fringing in Fig. 1c, magnetite produced by these procedures is highly crystalline.

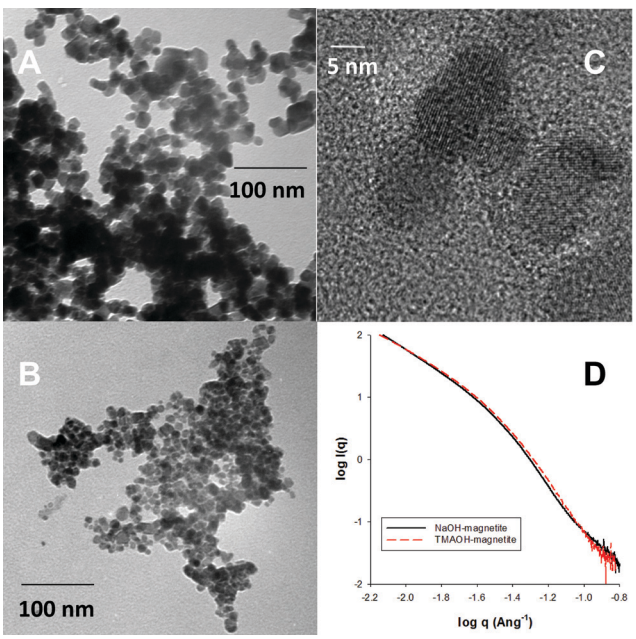

Fig. 1 A and B) TEM images of NaOH-magnetite and TMAOH-magnetite, respectively. C) HRTEM image of TMAOH magnetite, D) SAXS characterization of NaOH- and TMAOH-magnetite.

SAXS measurements were conducted to further characterize the primary nanoparticle size. As shown in Fig. 1d, the point at which there is an inflection in the Porod regime indicates a primary particle radius of 2.2 nm for NaOH-magnetite and 2.1 nm for TMAOH-magnetite. These values are smaller than the TEM determined size and we attribute this fact to the presence of small (<3 nm) nanoparticles that are detectable by SAXS, but are at the lower limit of our TEM imaging.

Magnetite cluster characterization

In both the NaOH-magnetite and TMAOH-magnetite suspensions, magnetite is present in the form of clusters of nanoparticles with DLS determined hydrodynamic radii varying from 100–200 to <30 nm, respectively (results not shown). These clusters, which presumably formed during nanomaterial synthesis, were highly resistant to disaggregation *via* bath sonication or solution agitation. Although the nucleation events leading to nanoparticle formation were rapid enough to ensure a small particle size,[30] the high-salt concentration conditions used during synthesis were such that electrical double layer repulsion was minimal and the particles immediately aggregated. Many existing references describing nanoparticle syntheses report cluster sizes that are considerably larger than the nascent nanoparticle size.[35]

The smaller cluster size of TMAOH-magnetite is attributed to the presence of the TMA^+ cation at the nanoparticle surface. This surface associated cation electrosterically restricts particle–particle interactions and facilitates nanoparticle dispersion.[36] The persistence of the adhered TMA^+ layer was found to be a function of the number of wash cycles employed to clean the nanoparticles following synthesis. Sequential wash steps resulted in an increase in the measured hydrodynamic radius for TMAOH-magnetite. Immediately following synthesis, the measured hydrodynamic radius was 18 nm (≈4.5× larger than the TEM determined individual particle radius), but depletion of surface associated TMA^+ following four additional wash cycles increased the measured radius to 30 nm (≈7.5× larger than the individual particle radius). As determined *via* ImageJ analysis of collected TEM images, these sequential washes did not statistically alter the intrinsic nanoparticle diameter (results not shown). In the experiments described herein, at least four wash steps were employed.

The surface charge of the nanomagnetite suspensions was determined as a function of the solution pH. The pH_{IEP} – or the pH where the measured zeta potential of the nanoparticle clusters was zero – was 6.8 ± 0.3 for NaOH-magnetite and 6.6 ± 1.0 for TMAOH-magnetite (Fig. 2a). These values are not statistically different and are within the range of pH_{IEP} values previously reported for magnetite.[36,37] Below the pH_{IEP} the surface is positively charged, while above the pH_{IEP} the surface is negatively charged. The slightly lower (but not statistically significant) pH_{IEP} for TMAOH-magnetite is consistent with the presence of adsorbed TMA^+ cations at the iron oxide surface. The complexation of organic materials at an oxide surface generally results in a lowering of the measured pH_{IEP}.[37]

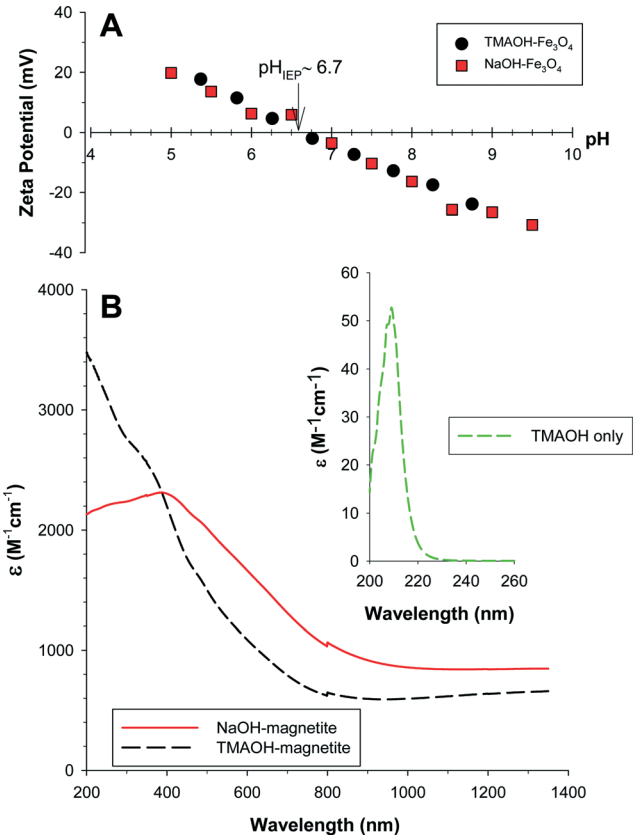

Fig. 2 A) Zeta potential as a function of solution pH for NaOH- and TMAOH-magnetite, 0.01 M NaCl was used as an indifferent electrolyte. B) Extinction spectra for NaOH- and TMAOH-magnetite. Inset: Extinction of TMAOH. [Note: the disconnect at ≈800 nm is due to a change in the instrument detector.]

Magnetite has a nondescript UV-vis-NIR spectrum consisting of overlapping absorption bands that are indicative of electronic transitions within the crystalline lattice. These transitions primarily result from 1) Fe^{III} ligand field effects, 2) interactions between magnetically coupled Fe^{III} ions, and 3) ligand (oxygen)–metal charge transfer excitations from the O(2p) non-bonding valence bands to the Fe(3d) ligand field orbitals or possibly between electron donor Fe^{II} and electron acceptor Fe^{III}.[38] The Fe^{III} ligand field transitions within magnetite primarily result in absorbance between 290–380 nm, while charge transfer transitions are responsible for the majority of the absorption in the visible-region of the spectra.[38] Magnetite also has an absorption maximum in the NIR region around 1500 nm due to electron hopping between octahedral Fe^{II} and Fe^{III} (*i.e.*, an intervalence charge transfer band [IVCT]).

Fig. 2b exhibits the UV-vis-NIR extinction (= absorption + scattering) spectra for NaOH-magnetite and TMAOH-magnetite. TMAOH-magnetite has higher extinction in the UV region than NaOH-magnetite, while in the near-IR it is lower. The former effect is attributed to the absorbance of the TMA^+ cations (Fig. 2b inset), while the latter could be the result of the decreased particle size for TMAOH-magnetite or to its

smaller cluster size. Each of these possibilities would result in less light extinction for a given mass of particles. Two extinction maxima in the magnetite spectrum exist over this wavelength range – one centered at 380 nm corresponding to Fe^{III} ligand field transitions and another at $\lambda > 1320$ nm that corresponds to the IVCT band.[39]

During storage the magnetite stock suspensions, particularly NaOH-magnetite, aggregate significantly. To breakup these agglomerates and attain a stable initial cluster size the experimental solutions were bath sonicated prior to each experiment. As shown in Fig. S2 in the ESI,† the initial absorbance at 508 nm of a magnetite suspension varies with both the sonication time and the particle concentration. Based upon these results, a presonication period of three minutes was chosen for all experiments described herein.

Collected SAXS scattering curves were analyzed and fit to determine a d_f of 1.88 ± 0.10 for NaOH-magnetite and a d_f of 1.79 ± 0.09 for TMAOH-magnetite. The lower d_f for TMAOH-magnetite indicates that the TMAOH-magnetite clusters exhibit a less densely packed structure, while NaOH-magnetite is more tightly packed. Both values indicate that these clusters formed *via* DLCA.

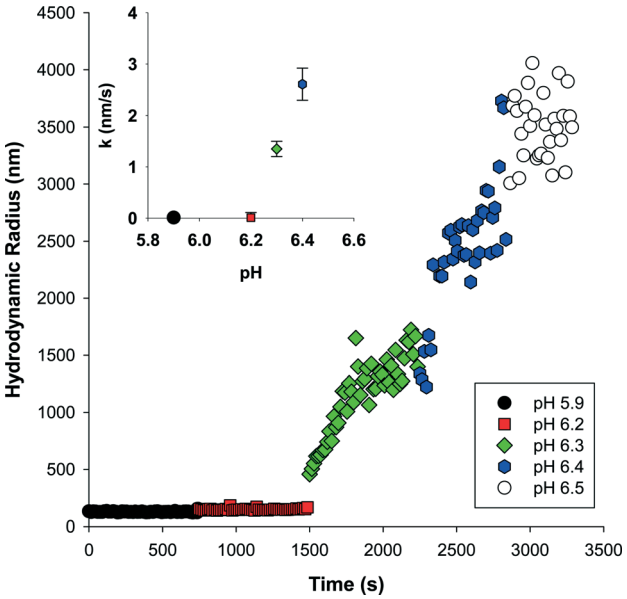

Fig. 3 Effect of solution pH on the aggregation of 0.012 mM NaOH-magnetite. Aliquots of 0.1 M NaOH were sequentially added to set the solution pH. Inset: Initial aggregation rate constants; error bars reflect the standard error.

Magnetite cluster–cluster aggregation

We evaluated the aggregation behavior of our magnetite clusters as dictated by solution pH and the presence of electrolytes. Cluster–cluster aggregation led to an increase in hydrodynamic radius that was quantified using DLS.

pH effects. To illustrate the effect of pH on cluster–cluster aggregation, we sequentially added aliquots of 0.1 M NaOH to a 0.012 mM NaOH-magnetite suspension (2.73 mg L^{-1}; 10^{15} nanoparticles L^{-1}) and then measured the hydrodynamic radius of the suspension over time to determine apparent aggregation rate constants (Fig. 3). Prior to base addition, the hydrodynamic radius was 130 ± 7 nm at a pH of 5.9. Increasing the pH to 6.2 resulted in a negligible increase in the hydrodynamic radius. An increase to pH 6.3 and beyond accelerated cluster–cluster aggregation and increased the measured hydrodynamic radius. At both pH 6.3 and pH 6.4 the change in the hydrodynamic radius was initially quite rapid ($k_{pH=6.3}$ = 1.4 nm s^{-1}, $k_{pH=6.4}$ = 2.6 nm s^{-1}). At pH 6.5, the first four readings exhibited a slope ($k_{pH=6.5}$) in excess of 10 nm s^{-1}, but became unstable thereafter as the overall cluster size approached the maximum limit of the DLS instrument employed. (We note that we utilize units of nm s^{-1} for simplicity. To determine the correct units for nanoparticle aggregation (*i.e.*, nm s^{-1}) we would need to assume volumes for the aggregating clusters.) The aggregation behavior shown in Fig. 3 is consistent with past studies examining the aggregation of nanoparticles and nanoparticle clusters.[27,40,41] The rate of change in the hydrodynamic radius of the cluster increased as the pH approached the pH_{IEP} of NaOH-magnetite. This behavior is consistent with colloid theory that suggests that at the isoelectric point the clusters will aggregate most rapidly due to the decreased thickness of the repulsive electrostatic double layer.[42]

Indifferent electrolyte effects. We investigated the salt induced aggregation of our NaOH- and TMAOH-magnetite clusters. Fig. S3† depicts illustrative results for the aggregation of NaOH-magnetite following NaCl addition. As expected, at low salt concentrations the kinetics of aggregation are quite slow. At higher salt concentrations, however, the aggregation kinetics accelerate. To quantify magnetite cluster–cluster aggregation we monitored the aggregation kinetics for t > 15 seconds to determine the aggregation rate constant:[27,42]

$$\left(\frac{dN_1}{dt}\right)_{t\to 0} = -k_{11}N_0^2 \quad (3)$$

where k_{11} is the measured aggregation rate constant obtained by fitting a linear regression to DLS acquired hydrodynamic data. N_0 is the concentration of nanomagnetite clusters at time t = 0 and N_1 is a dimer formed by aggregation of two clusters. Under high salt conditions where aggregation is limited only by the diffusion of two clusters (DLCA) the value of k_{11} is maximized and is defined as $k_{11,fast}$. For conditions where repulsive interactions control aggregation (RLCA) k_{11} is slower. We defined the stability of a suspension using the stability ratio W:

$$W = \frac{k_{11,fast}}{k_{11}} \quad (4)$$

After applying eqn (4) to our collected DLS data we plotted the stability ratio for NaOH-magnetite and TMAOH-magnetite *versus* salt concentration for three different salts (NaCl, $MgCl_2$, and $CaCl_2$) in Fig. 4a. As shown, the calculated stability ratios decrease with an increase in salt concentration up to a limiting value of 1. At salt levels in excess of this concentration, aggregation is limited only by diffusion since the

repulsive electrostatic energy barrier is diminished and further addition of salt no longer affects the aggregation rate. The salt concentration where this transition occurs is the critical coagulation concentration (CCC) and was experimentally determined by extrapolating the measured stability ratios at low salt concentrations to a value of 1. Using this approach, we determined approximate CCC values for our NaOH-magnetite clusters of: NaCl = 8 mM, $MgCl_2$ = 0.3 mM, and $CaCl_2$ = 0.2 mM. For the TMAOH-magnetite clusters the approximate CCC for NaCl was 5 mM. For NaOH-magnetite the difference between the results obtained with the monovalent and divalent cations is consistent with past reports and with the empirical Shulze–Hardy rule that predicts the CCC should scale with the sixth power of the valence.[24] The difference in CCC values for $CaCl_2$ *vs.* $MgCl_2$ is not statistically significant, but the data consistently show that NaOH-magnetite aggregates more rapidly in the presence of Ca^{2+} than at a comparable concentration of Mg^{2+}. Stankus *et al.*[43] recently reported that Ca^{2+} is more effective than Mg^{2+} at inducing aggregation of negatively charged AuNP, and they attributed this result to the fact that Ca^{2+} (electronegativity = 1.00 Pauling units) is slightly more electropositive than Mg^{2+} (1.31 Pauling units).

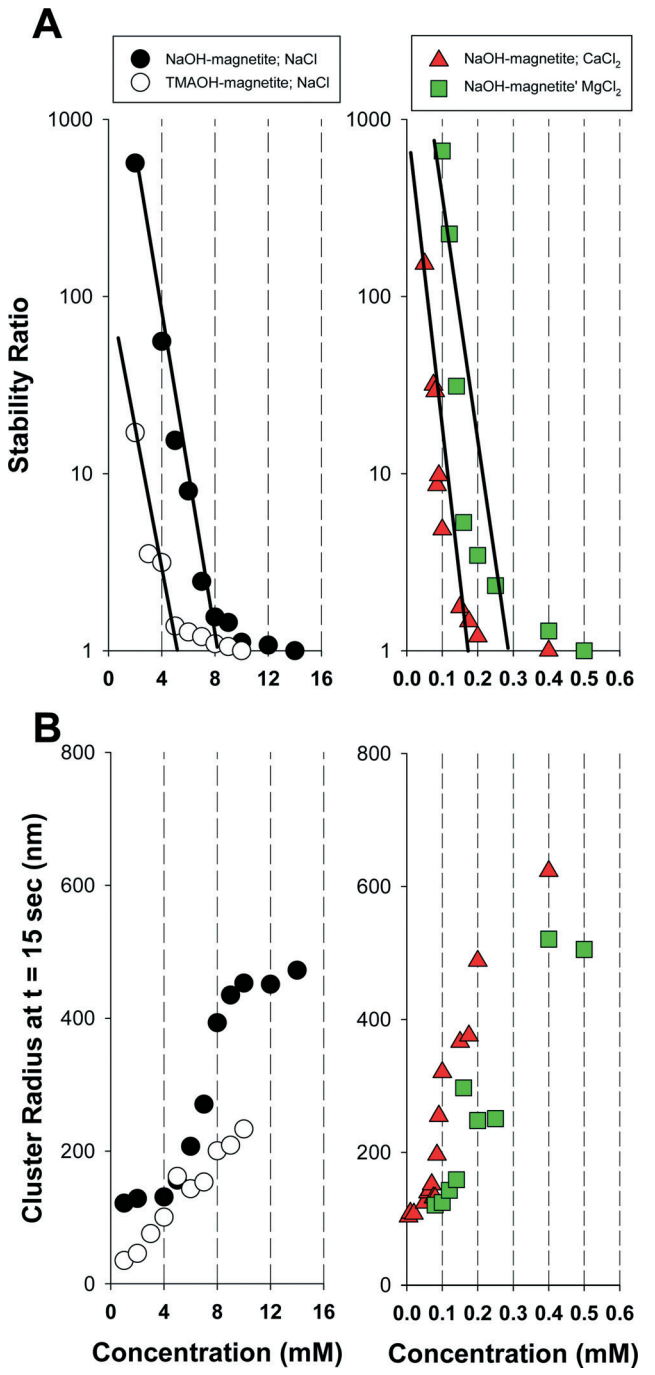

Fig. 4 A) Measured stability ratios for magnetite as a function of the salt concentration. B) Measured magnetite cluster radii at t = 15 s for the conditions in A). Magnetite = 0.012 mM. pH = 8.0 ± 0.5.

The most striking result presented in Fig. 4a is the lower observed CCC for TMAOH-magnetite than for NaOH-magnetite. Such a result is somewhat misleading, however, due to the smaller initial cluster size for TMAOH-magnetite than NaOH-magnetite. A smaller size cluster can be expected to aggregate more rapidly due to its higher overall rate of diffusion (which is inversely correlated to the cluster size). To illustrate the effects of salt on cluster size we present in Fig. 4b the measured cluster radius at t = 15 s (*i.e.*, the first DLS measurement obtained after salt addition). As shown, the TMAOH clusters are consistently smaller than those for NaOH-magnetite at similar salt concentrations.

It is possible to define the minimum salt concentration required to initiate cluster growth. As shown, in Fig. 4b (t = 15 s) and Fig. S4† (for t = 60, 90, 120 s), for NaOH-magnetite this condition occurs at salt concentrations of 4 mM NaCl, 0.08 mM $CaCl_2$, and 0.14 mM $MgCl_2$. For TMAOH-magnetite no minimum salt concentration could be defined over the NaCl range investigated, thus suggesting that cluster growth occurs at values below 1 mM. As expected, the concentrations at which cluster growth occurs are consistently lower than the measured CCC values.

Fe^{II} addition. In contrast to the aggregation behavior observed following addition of the indifferent electrolytes $CaCl_2$, $MgCl_2$, and NaCl, the addition of $FeCl_2$ resulted in a highly differential trend. It was observed that the suspension generally became more stable as indicated by a measured decrease in cluster size with an increase in Fe^{II} concentration (Fig. S5†). To our knowledge, the effects of Fe^{II} addition on iron based nanoparticle cluster stability have not been examined to date; however, Fe^{II} addition is expected to alter the surface properties of the magnetite nanoparticles, as has been suggested elsewhere.[44–47] A change in the oxidation state of magnetite, for example, may have produced clusters with higher colloidal stability than pristine nanomagnetite. The effects of changes in oxidation state on the stability of these nanomagnetite clusters will be the focus of a future publication.

Magnetite cluster sedimentation

An inherent problem with DLS is that the method requires low particle concentrations to prevent multiple scattering

events that lead to inaccurate light scattering measurements. Given this limitation, we examined the aggregation and sedimentation behavior of magnetite at higher nanoparticle concentrations by monitoring changes in optical absorbance as a function of time using UV-vis-NIR spectroscopy. Coagulation and sedimentation of the NaOH-magnetite and TMAOH-magnetite clusters was initiated by NaCl addition. Representative sets of sedimentation spectra are shown in Fig. 5. These spectra, obtained for NaOH-magnetite at a concentration of 0.864 mM (200 mg L^{-1}), illustrate that NaCl addition initiates the aggregation and sedimentation of the magnetite clusters. To probe magnetite sedimentation in greater temporal detail than enabled by full spectral monitoring we conducted a comprehensive series of experiments in which we monitored changes in absorbance at 508 nm over time. We selected this value for consistency with the literature[7] as well as the fact that the absorbance at this wavelength is not affected by the magnetite oxidation state. As documented previously, changes in oxidation state primarily affect the NIR portion of the UV-vis-NIR spectrum.[39]

The addition of salt at concentrations ranging from 2 to 20 mM caused a measurable decrease in absorption at 508 nm for both NaOH-magnetite (Fig. 6a) and TMAOH-magnetite (Fig. 6b). The detrimental effect of salt addition on the colloidal stability of magnetite was expected since an increase in the ionic strength of the solution lowers the repulsive electrostatic barrier and enables rapid coagulation. Relative to the salt-free suspension, the observed sedimentation kinetics were enhanced upon addition of ≥2 mM salt; however, there was no discernable trend observed in the sedimentation curves for salt concentrations between 2 and 20 mM (data not shown). This effect was surprising since we previously had shown using DLS (Fig. 4a) that the NaCl CCC for NaOH-magnetite was 8 mM and thus we had anticipated that there would be differences in the sedimentation curves obtained below the CCC (RLCA conditions) relative to those obtained above the CCC (DLCA conditions). It is possible that the higher magnetite concentrations used in the sedimentation studies may have masked the salt effects due to the higher mass loading. It would be expected, however, that the CCC should be invariant with changes in the mass load since it is defined as the point where the salt concentration exceeds that required to eliminate electrostatic repulsion between two interacting objects.

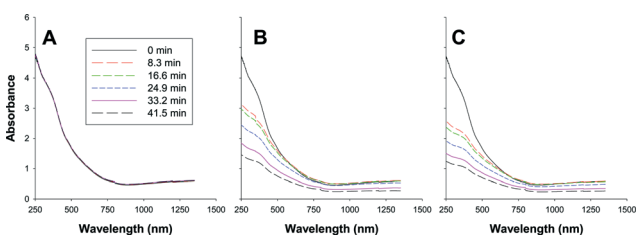

Fig. 5 Collected sedimentation curves for 0.864 mM NaOH-magnetite. A) No salt addition, B) 10 mM NaCl, C) 20 mM NaCl.

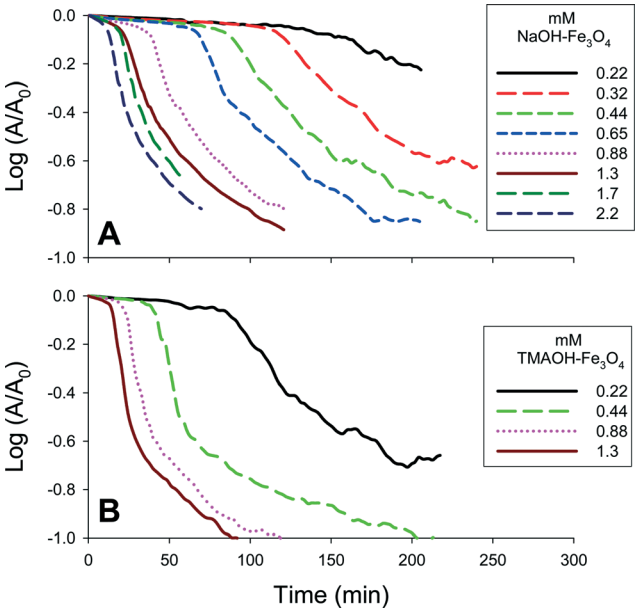

Fig. 6 Representative A) NaOH- and B) TMAOH-magnetite sedimentation curves obtained at 508 nm. The magnetite concentration was varied between 0.22–2.2 mM (50–500 mg L^{-1}). A fixed concentration of 10 mM NaCl was used to induce sedimentation.

The collected sedimentation curves can be subdivided into three regions that are demarcated by changes in slope (Fig. S6†).[7] The first region (aggregation I) corresponds to the initial coagulation of the magnetite clusters. In this region, the clusters are coagulating, but have not reached the critical size needed to initiate rapid sedimentation. Once the critical size is reached, at time t_{crit1}, sedimentation occurs rapidly (sedimentation I). The kinetics of sedimentation are determined by calculating the slope of the collected results over this period. For some suspensions, particularly those with high salt and mass concentrations, a third region with a slower sedimentation rate can be observed (sedimentation II). This region, initiated at time t_{crit2}, has previously been interpreted as the sedimentation of clusters that failed to attain critical size.

As shown in Fig. 6 and summarized in Table S1,† changes in magnetite concentration systematically altered the measured rates of aggregation and sedimentation. Sedimentation experiments were performed using magnetite suspensions with concentrations ranging from 0.22–2.2 mM (50–500 mg L^{-1}) and NaCl concentrations ranging from 0–30 mM. The apparent aggregation rates were obtained by determining the slope of the change in absorbance measured at 508 nm, over time up to t_{crit1}.

A direct relationship between particle concentration and aggregation rate is shown in Fig. 7a and b. As shown, the effect of particle concentration was significant for each tested salt concentration and, as noted previously, there was little difference in the aggregation kinetics measured for 10–30 mM NaCl.

At the lowest mass concentrations tested (0.22 and 0.43 mM), TMAOH-magnetite clusters aggregate more rapidly than

NaOH-magnetite, as evinced by their relative k_{agg} values, while at the higher mass concentrations (0.86 and 1.3 mM), the opposite is true. The former result is consistent with the DLS results presented in Fig. 4a that suggested that TMAOH-magnetite aggregates more rapidly, while the latter result is inconsistent with the DLS results. For low magnetite concentrations the TMAOH-magnetite clusters aggregate more quickly and reach the critical size required to initiate settling more rapidly. To illustrate this effect, we plotted the variation in t_{crit1} as a function of the magnetite concentration (Fig. S7†). As illustrated, TMAOH-magnetite consistently has a lower t_{crit1} value than NaOH-magnetite. Furthermore, for both NaOH-magnetite and TMAOH-magnetite higher initial concentrations require increasingly shorter aggregation times to reach the critical size required for settling. The t_{crit1} values appear to plateau at high magnetite concentrations, thereby suggesting that above a certain mass concentration, cluster sedimentation is initiated at a fixed point in time. As shown in Fig. S7,† such a plateau is consistent with the experimental results of Phenrat *et al.*[7]

For a given mass concentration, the measured rate constants (k_{SED1}) for the settling of TMAOH-magnetite during the sedimentation I period are generally higher than those for NaOH-magnetite. Such a result, and the observed trends in the aggregation rates, are consistent with the lower fractal dimension of the TMAOH-magnetite clusters. In the following section we examine how the different d_f values for NaOH-magnetite and TMAOH-magnetite alter their respective sedimentation rates.

Mathematical evaluation of cluster sedimentation

Based upon the fractal dimension it is possible to estimate the expected settling velocity (u^*) for a fractal cluster. This can be done using a modified form of Stokes law:[22,48]

$$u^* = \frac{\left(\rho_{magnetite} - \rho_{water}\right) g \Phi d^2}{18 \mu \Omega} \quad (5)$$

where g is the acceleration due to gravity, $\rho_{magnetite}$ is the density of magnetite (4.95 g cm^{-3}), ρ_{water} is the density of water (0.998 g cm^{-3}), d is the cluster diameter, ϕ is the volumic fraction (= 10^{-5}–10^{-4}), and Ω is the ratio between the drag force on a permeable aggregate and the drag force on an impermeable aggregate. This ratio can be calculated as:

$$\Omega = \frac{2\xi^2\left(1 - \frac{\tanh \xi}{\xi}\right)}{2\xi^2 + 3\left(1 - \frac{\tanh \xi}{\xi}\right)} \quad (6)$$

where, ξ is the non-dimensional permeability:

$$\xi = \frac{d}{2\sqrt{K}} \quad (7)$$

For this effort, we estimated the cluster permeability (K) using the Happel cell model:

$$K = \frac{2a_p^{\,2}}{9\rho} \frac{\left(3 - 4.5\rho^{1/3} + 4.5\rho^{5/3} - 3\rho^2\right)}{\left(3 + 2\rho^{5/3}\right)} \quad (8)$$

where ρ is the cluster density and is based upon the individual nanoparticle radius (a_p) as well as the measured fractal dimension:

$$\rho = c\left(\frac{d}{2a_p}\right)^{d_f - 3} \quad (9)$$

where c is the packing density (assumed to be 0.1). Using the model defined by eqn (5)–(9), and our SAXS determined d_f values, we calculated expected settling velocities for various size clusters of NaOH-magnetite and TMAOH-magnetite. As shown in Fig. 8, the TMAOH-magnetite clusters are expected to sediment at rates slightly faster than NaOH-magnetite clusters of the same size. Furthermore, due to their fractal and thus porous nature, both types of clusters sediment at rates considerably larger than an impermeable sphere of the same size. This result is qualitatively consistent with the data in Fig. 7 and Table S1† with slightly higher sedimentation rates for TMAOH-magnetite than for NaOH-magnetite of comparable cluster size.

We note that the simple model defined by eqn (5)–(9) provides insight into how the fractal dimension of a nanoparticle cluster affects its settling rate, but does not consider the complicating effects of cluster restructuring[48] that are expected to occur during aggregation and/or sedimentation. Such restructuring would alter the fractal dimension and thus the dynamics of nanoparticle cluster settling may be considerably more complex than illustrated herein. Therefore for this reason, we refrain from making direct comparison of our experimental and model results. Collectively, however,

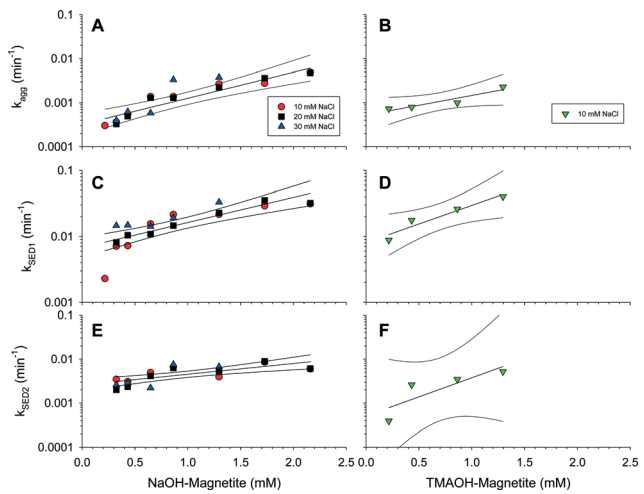

Fig. 7 Experimentally determined k_{agg}, k_{SED1}, and k_{SED2} rate constants for NaOH-magnetite (A, C, E) and TMAOH-magnetite (B, D, F). The magnetite mass concentrations varied from 0.22–2.2 mM (50–500 mg L^{-1}). Curves reflect the best fit line and the 95% confidence limits.

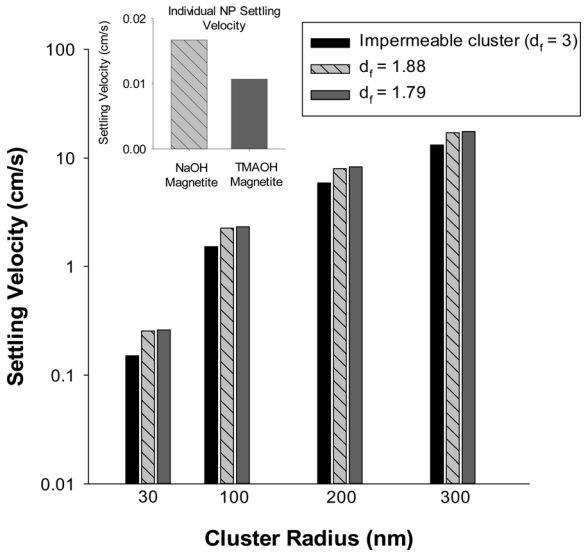

Fig. 8 Effects of fractal dimension and cluster radius on the sedimentation constants for magnetite. As the fractal dimension increases there is an expected decrease in settling velocity. For all conditions tested, for a given cluster size TMAOH-magnetite settles more rapidly than NaOH-magnetite. Inset: When present as individual nanoparticles NaOH-magnetite (5 nm radius) is expected to sediment more rapidly than TMAOH-magnetite (4 nm radius) due to its larger size.

the experimental and model results shown here clearly indicate the important, yet often overlooked role of fractal dimension in nanoparticle aggregation and settling.

Conclusions

Following salt addition, and in the absence of stabilizers, magnetite clusters aggregate and readily settle out of suspension. The rates of aggregation and sedimentation are dependent on particle concentration and aqueous conditions such as pH and ionic strength. These factors have historically been considered to be the primary ones that dictate the fate of magnetite and other nanoparticles in natural and engineered systems. As documented, herein, however the fractal dimension of the aggregating and sedimenting clusters must also be considered. As shown, simple measurements of nanoparticle aggregation are insufficient to predict removal rates for suspended nanoparticles. A combination of aggregation, sedimentation, and fractal dimension measurements are collectively required to enable accurate predictions of nanoparticle fate.

Acknowledgements

This material is based upon work supported by the National Science Foundation (NSF) and the Environmental Protection Agency (EPA) under NSF Cooperative Agreement EF-0830093, Center of the Environmental Implications of NanoTechnology (CEINT). Any opinions, findings, conclusions or recommendations expressed in this material are those of the author(s) and do not necessarily reflect the views of the NSF or the EPA. This work has not been subjected to EPA review and no official endorsement should be inferred. Additional funding was provided by the National Science Foundation (CBET-0537117) and the Labex Serenade (no ANR-11-LABX-0064) funded by the "Investissements d'Avenir" French Government program of the French National Research Agency (ANR) through the A*MIDEX project (no ANR-11-\-02).

References

1 A. F. White, M. L. Peterson and M. F. Hochella, Electrochemistry and dissolution kinetics of magnetite and ilmenite, *Geochim. Cosmochim. Acta*, 1994, **58**(8), 1859–1875.
2 A. F. White and M. L. Peterson, Reduction of aqueous transition metal species on the surfaces of Fe(II)-containing oxides, *Geochim. Cosmochim. Acta*, 1996, **60**(20), 3799–3814.
3 T. Kohn, K. J. T. Livi, A. L. Roberts and P. J. Vikesland, Longevity of granular iron in groundwater treatment processes: Corrosion product development, *Environ. Sci. Technol.*, 2005, **39**(8), 2867–2879.
4 S. Glasauer, S. Langley and T. J. Beveridge, Intracellular iron minerals in a dissimilatory iron-reducing bacterium, *Science*, 2002, **295**(5552), 117–119.
5 D. R. Lovley and E. J. P. Phillips, Novel mode of microbial energy metabolism - organic-carbon oxidation coupled to dissimilatory reduction of iron or manganese, *Appl. Environ. Microbiol.*, 1988, **54**(6), 1472–1480.
6 I. Medvedeva, Y. Bakhteeva, S. Zhakov, A. Revvo, I. Byzov, M. Uimin, A. Yermakov and A. Mysik, Sedimentation and aggregation of magnetite nanoparticles in water by a gradient magnetic field, *J. Nanopart. Res.*, 2013, **15**(11), DOI: 10.1007/s11051-013-2054-y.
7 T. Phenrat, N. Saleh, K. Sirk, R. D. Tilton and G. V. Lowry, Aggregation and sedimentation of aqueous nanoscale zerovalent iron dispersions, *Environ. Sci. Technol.*, 2007, **41**(1), 284–290.
8 N. Savage and M. S. Diallo, Nanomaterials and water purification: Opportunities and challenges, *J. Nanopart. Res.*, 2005, **7**(4–5), 331–342.
9 S. C. N. Tang and I. M. C. Lo, Magnetic nanoparticles: Essential factors for sustainable environmental applications, *Water Res.*, 2013, **47**(8), 2613–2632.
10 P. J. Vikesland, A. M. Heathcock, R. L. Rebodos and K. E. Makus, Particle size and aggregation effects on magnetite reactivity toward carbon tetrachloride, *Environ. Sci. Technol.*, 2007, **41**(15), 5277–5283.
11 W. Yantasee, C. L. Warner, T. Sangvanich, R. S. Addleman, T. G. Carter, R. J. Wiacek, G. E. Fryxell, C. Timchalk and M. G. Warner, Removal of heavy metals from aqueous systems with thiol functionalized superparamagnetic nanoparticles, *Environ. Sci. Technol.*, 2007, **41**(14), 5114–5119.
12 C. T. Yavuz, J. T. Mayo, W. W. Yu, A. Prakash, J. C. Falkner, S. Yean, L. Cong, H. J. Shipley, A. Kan, M. Tomson, D. Natelson and V. L. Colvin, Low-field magnetic separation of monodisperse Fe_3O_4 nanocrystals, *Science*, 2006, **314**(5801), 964–967.

13 M. L. McCormick, E. J. Bouwer and P. Adriaens, Carbon tetrachloride transformation in a model iron-reducing culture: Relative kinetics of biotic and abiotic reactions, *Environ. Sci. Technol.*, 2002, **36**(3), 403–410.

14 R. L. Rebodos and P. J. Vikesland, Effects of oxidation on the magnetization of nanoparticulate magnetite, *Langmuir*, 2010, **26**(22), 16745–16753.

15 Y. Lu, Y. D. Yin, B. T. Mayers and Y. N. Xia, Modifying the surface properties of superparamagnetic iron oxide nanoparticles through a sol–gel approach, *Nano Lett.*, 2002, **2**(3), 183–186.

16 L. A. Harris, J. D. Goff, A. Y. Carmichael, J. S. Riffle, J. J. Harburn, T. G. St Pierre and M. Saunders, Magnetite nanoparticle dispersions stabilized with triblock copolymers, *Chem. Mater.*, 2003, **15**(6), 1367–1377.

17 C. T. Yavuz, J. T. Mayo, S. Yean, L. Cong, W. Yu, J. Falkner, A. Kan, M. Tomson and V. L. Colvin, in *Particle size dependence of nano-magnetite in arsenic removal*, ed. F. Kongoli and R. G. Reddy, Sohn International Symposium on Advanced Processing of Metals and Materials, San Diego, CA, Aug 27–31, 2006; C. T. Yavuz, J. T. Mayo, S. Yean, L. Cong, W. Yu, J. Falkner, A. Kan, M. Tomson and V. L. Colvin, in *Particle size dependence of nano-magnetite in arsenic removal*, ed. F. Kongoli and R. G. Reddy, Minerals, Metals & Materials Soc, San Diego, CA, 2006, pp. 221–228.

18 G. Rubasinghege, R. W. Lentz, H. Park, M. M. Scherer and V. H. Grassian, Nanorod dissolution quenched in the aggregated state, *Langmuir*, 2010, **26**(3), 1524–1527.

19 M. Y. Lin, H. M. Lindsay, D. A. Weitz, R. C. Ball, R. Klein and P. Meakin, Universality in colloid aggregation, *Nature*, 1989, **339**(6223), 360–362.

20 G. Nichols, S. Byard, M. J. Bloxham, J. Botterill, N. J. Dawson, A. Dennis, V. Diart, N. C. North and J. D. Sherwood, A review of the terms agglomerate and aggregate with a recommendation for nomenclature used in powder and particle characterization, *J. Pharm. Sci.*, 2002, **91**(10), 2103–2109.

21 B. E. Logan and J. R. Kilps, Fractal dimensions of aggregates formed in different fluid mechanical environments, *Water Res.*, 1995, **29**(2), 443–453.

22 X. Y. Li and B. E. Logan, Collision frequencies of fractal aggregates with small particles by differential sedimentation, *Environ. Sci. Technol.*, 1997, **31**(4), 1229–1236.

23 P. Meakin, Fractal aggregates, *Adv. Colloid Interface Sci.*, 1987, **28**, 249–331.

24 P. C. Hiemenz, *Principles of colloid and surface chemistry*, Marcel Dekker Inc., New York, New York, 3rd edn, 1997.

25 P. Sandkuhler, M. Lattuada, H. Wu, J. Sefcik and M. Morbidelli, Further insights into the universality of colloidal aggregation, *Adv. Colloid Interface Sci.*, 2005, **113**(2–3), 65–83.

26 M. Berka and J. A. Rice, Relation between aggregation kinetics and the structure of kaolinite aggregates, *Langmuir*, 2005, **21**(4), 1223–1229.

27 S. E. Mylon, K. L. Chen and M. Elimelech, Influence of natural organic matter and ionic composition on the kinetics and structure of hematite colloid aggregation: Implications to iron depletion in estuaries, *Langmuir*, 2004, **20**(21), 9000–9006.

28 B. A. Chambers, A. Afrooz, S. Bae, N. Aich, L. Katz, N. B. Saleh and M. J. Kirisits, Effects of chloride and ionic strength on physical morphology, dissolution, and bacterial toxicity of silver nanoparticles, *Environ. Sci. Technol.*, 2014, **48**(1), 761–769.

29 R. Pamies, J. G. H. Cifre, V. F. Espin, M. Collado-Gonzalez, F. G. D. Banos and J. G. de la Torre, Aggregation behaviour of gold nanoparticles in saline aqueous media, *J. Nanopart. Res.*, 2014, **16**(4), DOI: 10.1007/s11051-014-2376-4.

30 L. Vayssières, C. Chaneac, E. Tronc and J. P. Jolivet, Size tailoring of magnetite particles formed by aqueous precipitation: An example of thermodynamic stability of nanometric oxide particles, *J. Colloid Interface Sci.*, 1998, **205**(2), 205–212.

31 A. Masion, D. Tchoubar, J. Y. Bottero, F. Thomas and F. Villieras, Chemistry and structure of Al(OH)/organic precipitates - a small-angle x-ray-scattering study. 1. Numerical procedure for speciation from scattering curves, *Langmuir*, 1994, **10**(11), 4344–4348.

32 A. Masion, J. Y. Bottero, F. Thomas and D. Tchoubar, Chemistry and structure of Al(OH)/organic precipitates - a small-angle x-ray-scattering study. 2. Speciation and structure of the aggregates, *Langmuir*, 1994, **10**(11), 4349–4352.

33 A. Afrooz, I. A. Khan, S. M. Hussain and N. B. Saleh, Mechanistic heteroaggregation of gold nanoparticles in a wide range of solution chemistry, *Environ. Sci. Technol.*, 2013, **47**(4), 1853–1860.

34 I. A. Khan, A. Afrooz, J. R. V. Flora, P. A. Schierz, P. L. Ferguson, T. Sabo-Attwood and N. B. Saleh, Chirality affects aggregation kinetics of single-walled carbon nanotubes, *Environ. Sci. Technol.*, 2013, **47**(4), 1844–1852.

35 A. R. Petosa, D. P. Jaisi, I. R. Quevedo, M. Elimelech and N. Tufenkji, Aggregation and deposition of engineered nanomaterials in aquatic environments: Role of physicochemical interactions, *Environ. Sci. Technol.*, 2010, **44**(17), 6532–6549.

36 S. C. Pang, S. F. Chin and M. A. Anderson, Redox equilibria of iron oxides in aqueous-based magnetite dispersions: Effect of pH and redox potential, *J. Colloid Interface Sci.*, 2007, **311**(1), 94–101.

37 U. Schwertmann and R. M. Cornell,in *The iron oxides: Structure, properties, reactions, occurrence and uses*, VCH, Weinheim, Germany, 1996.

38 R. M. Cornell and U. S. Schwertmann, *The iron oxides structure, properties, reactions, occurrences and uses*, Wiley-VCH Verlag GmbH & Co. KGaA, Weinheim, 2nd edn, 2003, p. 664.

39 J. Tang, M. Myers, K. A. Bosnick and L. E. Brus, Magnetite Fe_3O_4 nanocrystals: Spectroscopic observation of aqueous oxidation kinetics, *J. Phys. Chem. B*, 2003, **107**(30), 7501–7506.

40 K. L. Chen, S. E. Mylon and M. Elimelech, Enhanced aggregation of alginate-coated iron oxide (hematite) nanoparticles in the presence of calcium, strontium, and barium cations, *Langmuir*, 2007, **23**(11), 5920–5928.

41 R. A. French, A. R. Jacobson, B. Kim, S. L. Isley, R. L. Penn and P. C. Baveye, Influence of ionic strength, pH, and cation valence on aggregation kinetics of titanium dioxide nanoparticles, *Environ. Sci. Technol.*, 2009, **43**(5), 1354–1359.

42 M. Elimelech, J. Gregory, X. Jia and R. A. Williams, *Particle deposition and aggregation: Measurment, modelling and simulation*, Butterworth-Heinemann, Woburn, MA, 1995.
43 D. Stankus, S. Lohse, J. Hutchison and J. Nason, Interactions between natural organic matter and gold nanoparticles stabilized with different organic capping agents, *Environ. Sci. Technol.*, 2010, **45**, 3238–3244.
44 C. A. Gorski, J. T. Nurmi, P. G. Tratnyek, T. B. Hofstetter and M. M. Scherer, Redox behavior of magnetite: Implications for contaminant reduction, *Environ. Sci. Technol.*, 2010, **44**(1), 55–60.
45 C. A. Gorski and M. M. Scherer, Influence of magnetite stoichiometry on fe-ii uptake and nitrobenzene reduction, *Environ. Sci. Technol.*, 2009, **43**(10), 3675–3680.
46 D. E. Latta, C. A. Gorski, M. I. Boyanov, E. J. O'Loughlin, K. M. Kemner and M. M. Scherer, Influence of magnetite stoichiometry on U^{VI} reduction, *Environ. Sci. Technol.*, 2012, **46**(2), 778–786.
47 T. S. Pasakarnis, M. I. Boyanov, K. M. Kemner, B. Mishra, E. J. O'Loughlin, G. Parkin and M. M. Scherer, Influence of chloride and Fe(II) content on the reduction of Hg(II) by magnetite, *Environ. Sci. Technol.*, 2013, **47**(13), 6987–6994.
48 A. Thill, S. Moustier, J. Aziz, M. R. Wiesner and J. Y. Bottero, Flocs restructuring during aggregation: Experimental evidence and numerical simulation, *J. Colloid Interface Sci.*, 2001, **243**(1), 171–182.